Final-state interactions in two-nucleon knockout reactions

Camille Colle,* Wim Cosyn,† and Jan Ryckebusch‡

Department of Physics and Astronomy,

Ghent University, Proeftuinstraat 86, B-9000 Gent, Belgium

(Dated: December 25, 2015)

Background: Exclusive two-nucleon knockout after electroexcitation of nuclei ($A(e,e'NN)$ in brief) is considered to be a primary source of information about short-range correlations (SRC) in nuclei. For a proper interpretation of the data, final-state interactions (FSI) need to be theoretically controlled.

Purpose: Our goal is to quantify the role of FSI effects in exclusive $A(e,e'pN)$ reactions for four target nuclei representative for the whole mass region. Our focus is on processes that are SRC driven. We investigate the role of FSI for two characteristic detector setups corresponding with a "small" and "large" coverage of the available phase space.

Method: Use is made of a factorized expression for the $A(e,e'pN)$ cross section that is proportional to the two-body center-of-mass (c.m.) momentum distribution of close-proximity pairs. The $A(e,e'pp)$ and $A(e,e'pn)$ reactions for the target nuclei ^{12}C, ^{27}Al, ^{56}Fe and ^{208}Pb are investigated. The elastic attenuation mechanisms in the FSI are included using the relativistic multiple-scattering Glauber approximation (RMSGA). Single-charge exchange (SCX) reactions are also included. We introduce the nuclear transparency T_A^{pN}, defined as the ratio of exclusive $(e,e'pN)$ cross sections on nuclei to those on "free" nucleon pairs, as a measure for the aggregated effect of FSI in pN knockout reactions from nucleus A. A toy model is introduced in order to gain a better understanding of the A dependence of T_A^{pN}.

Results: The transparency T_A^{pN} drops from $0.2-0.3$ for ^{12}C to $0.04-0.07$ for ^{208}Pb. For all considered kinematics, the mass dependence of the T_A^{pN} can be captured by the power law $T_A^{pN} \propto A^{-\lambda}$ with $0.4 \lesssim \lambda \lesssim 0.5$. Apart from an overall reduction factor, we find that FSI only modestly affects the distinct features of SRC-driven $A(e,e'pN)$ which are dictated by the c.m. distribution of close-proximity pairs.

Conclusion: The SCX mechanisms represent a relatively small (order of a few percent) contribution of SRC-driven $A(e,e'pN)$ processes. The mass dependence of FSI effects in exclusive $A(e,e'pN)$ can be captured in a robust power law and is in agreement with the predictions obtained in a toy model.

PACS numbers: 25.30.Rw, 25.30.Fj, 24.10.i

arXiv:1512.07841v1 [nucl-th] 24 Dec 2015

* Camille.Colle@UGent.be

† Wim.Cosyn@UGent.be

‡ Jan.Ryckebusch@UGent.be

I. INTRODUCTION

Nuclear SRC are an essential ingredient of the dynamics of nuclei at large momenta and energies. The short- and medium-range components of the nucleon-nucleon interaction induce beyond mean-field high-momentum and high-density fluctuations in the nuclear medium, thereby giving rise to fat tails in the nuclear momentum distributions [1–3]. The magnitude of nuclear SRC has been linked to plateaus in ratios of cross sections of inclusive electron scattering off different nuclei [4–6], and to the size of the EMC effect [7].

Nuclear SRC can be studied in exclusive two-nucleon knockout processes with hadronic and electroweak probes. In appropriately selected kinematics, those reactions give access to the dynamics and isospin composition of the initial nucleon pair. In the 1990s, high-resolution $A(e,e'pp)$ measurements carried out at MAMI [8, 9] and NIKHEF [10–12] could determine the transition to a specific final state of the residual $A-2$ nucleus. When comparing to data for the ^{16}O$(e,e'pp)$ transition to the 0^+ ground state of ^{14}C, model calculations [13–15] showed the clear dominance of SRC contributions to the cross section at low c.m. pair momentum, where the initial pair is in a relative S-state. The EVA collaboration at Brookhaven National Laboratory (BNL) measured the ^{12}C(p,ppn) reaction [16] as a function of the initial neutron momentum. For neutron momenta above the Fermi surface (~ 220 MeV) the data showed a clear angular correlation between the initial proton and neutron momenta with backward angles ($> 90^\circ$) dominating. For momenta below the Fermi surface the angular correlation between the two nucleon momenta is almost random. This picture was later confirmed by a ^{3}He$(e,e'pp)$ experiment performed in Jefferson Lab [17]. More recently, ^{12}C$(e,e'pN)$ [18, 19] and ^{4}He$(e,e'pN)$ [20] measurements (both at Jefferson Lab) provided proof that in the probed kinematics about 20% of the nucleons in nuclei form correlated pairs. Of those, about 90% is of the proton-neutron type [21], illustrating the dominance of tensor correlations in the nucleon momentum region of 300-500 MeV/c. A feature that emerges from all those experimental investigations, is that SRC pairs are mostly in a back-to-back configuration with a high relative and small c.m. momentum, whereby small and large are defined relative to the Fermi momentum.

In this paper we focus on the effect of FSI in SRC-driven high-virtuality $A(e,e'pN)$ cross sections. In Sec. II, we discuss the approximations underlying the factorized form of the $A(e,e'pN)$ cross section (detailed in Ref. [22]) and how we implement the FSI. Using the factorized $A(e,e'pN)$ cross-section expression, we show in Sec. II C that cross-section ratios can be directly related to the ratios of the integrated distorted two-body c.m. momentum distributions of close-proximity nucleon pairs. In Sec. III, we apply the developed model to four different target nuclei (^{12}C, ^{27}Al, ^{56}Fe, ^{208}Pb) and two very different kinematics probing SRC pairs. First, the kinematics of the $A(e,e'pp)$ cross-section measurements with the CEBAF Large Acceptance Spectrometer (CLAS) [21] covering a very large phase space. Second, the kinematics of an experimental setup with a very restricted phase-space coverage [18]. We extract the nuclear transparencies for two-nucleon knockout and compare them to single-particle knockout transparencies extracted from $A(e,e'p)$ measurements. We propose parameterizations for the mass dependence of the $A(e,e'pN)$ transparencies in the form of a power law and study its robustness. The opening-angle distribution for the initial correlated nucleon pair is shown to be dominated by backward angles, with little modification after the inclusion of FSI. A toy model that captures the essential features of elastic attenuation mechanisms in $A(e,e'NN)$ is proposed. This toy model allows us to gain a more qualitative understanding of the mass dependence of the nuclear transparency. Conclusions are given in Sec. IV.

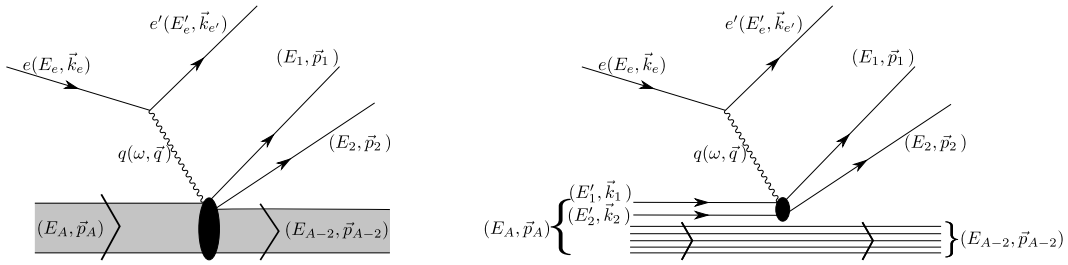

FIG. 1. (left) Sketch of the exclusive $A(e, e'pN)$ reaction with all kinematic variables. (right) The $A(e, e'pN)$ reaction in the impulse- and spectator approximation.

II. MODEL

A. Factorization of the $A(e, e'pN)$ cross section

We consider exclusive electroinduced knockout of a correlated proton-nucleon (pN) pair from the target nucleus A

$$e + A \to e' + (A-2)^* + p + N\,. \tag{1}$$

In this paper we solely deal with reactions whereby the residual $(A-2)^*$ is left with little or no excitation energy. This condition is essential for keeping the number of contributing reaction mechanisms under control.

Let $(\vec{k}_1, \vec{k}_2)$ and $(\vec{p}_1, \vec{p}_2)$ be the initial and final three-momenta of the nucleon pair. We label the struck proton with "1" and the recoiling nucleon with "2". In the impulse approximation, in which the exchanged momentum is absorbed by a single nucleon, we have that $\vec{p}_1 = \vec{k}_1 + \vec{q}$ with $\vec{q}$ the transferred three-momentum of the virtual photon (Fig. 1). We define the c.m. $\vec{P}_{12}$ and relative momentum $\vec{k}_{12}$ of the initial pair as,

$$\vec{P}_{12} = \vec{k}_1 + \vec{k}_2, \qquad \vec{k}_{12} = \frac{\vec{k}_1 - \vec{k}_2}{2}\,. \tag{2}$$

The corresponding c.m. and relative coordinates are denoted by $\vec{R}_{12}$ and $\vec{r}_{12}$.

By selecting events with a large $|\vec{q}|$ (large in comparison to the initial momenta $(\vec{k}_1, \vec{k}_2)$ of the nucleon pair) and requiring that one of the measured nucleons carries a significant fraction of the exchanged momentum $|\vec{q}|$, the contribution from the exchange term in which nucleon "2" absorbs the photon can be made negligible. Indeed, above the Fermi momentum, the $\vec{k}_{12}$ distribution of the pairs is strongly decreasing with increasing $|\vec{k}_{12}|$ [22, 23]. This makes it highly unlikely that the fast nucleon in the final state is not the one that absorbed the virtual photon.

As outlined in Refs. [22, 24], in kinematics probing SRC pairs, it is possible to factorize the $A(e, e'pN)$ cross section in a product of a function depending on the relative momentum $\vec{k}_{12}$, and a part depending on the c.m. momentum $\vec{P}_{12}$ of the initial pN pair

$$\frac{\mathrm{d}^8\sigma(e, e'pN)}{\mathrm{d}^2\Omega_{k_{e'}}\mathrm{d}^3\vec{p}_1\mathrm{d}^3\vec{p}_2} = \frac{M_A M_{A-2}}{E_A E_{A-2}}\frac{1}{(2\pi)^3} f_{\mathrm{rec}}\sigma_{epN}(\vec{k}_{12})F_A^{pN,D}(\vec{P}_{12})\,, \tag{3}$$

with $\Omega_{k_{e'}}$ the solid angle of the scattered electron, f_{rec} the recoil factor,

$$f_{\mathrm{rec}} = \frac{\left|1 - \frac{E_{e'}}{E_2}\frac{\vec{p}_2\cdot\vec{k}_{e'}}{|\vec{k}_{e'}|^2}\right|}{\left|1 + \frac{E_{e'}}{E_{A-2}}\frac{\vec{P}\cdot\vec{k}_{e'}}{|\vec{k}_{e'}|^2}\right|}\,, \tag{4}$$

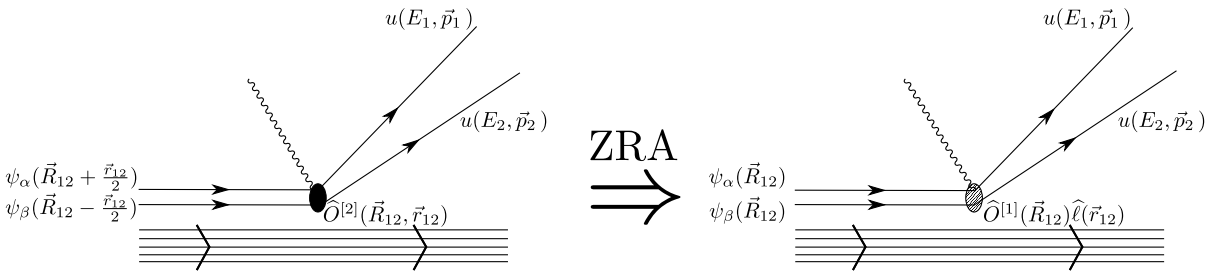

FIG. 2. A sketch of the zero-range approximation (ZRA) which underlies the factorized expression of the exclusive $A(e,e'pN)$ cross section.

and M_A, E_A (M_{A-2},E_{A-2}) the rest mass and energy of the initial (recoiling $A-2$) nucleus. $\sigma_{epN}(\vec{k}_{12})$ encodes the virtual-photon coupling to a correlated pN pair with relative momentum $\vec{k}_{12}$. $F_A^{pN,D}(\vec{P}_{12})$ is the distorted c.m. momentum distribution of the close-proximity pair that absorbs the photon. The factorized cross-section expression of Eq. (3) hinges on the validity of the zero-range approximation (ZRA), which amounts to putting the relative pair coordinate $\vec{r}_{12}$ to zero (Fig. 2). Thereby, the amplitude for photo-absorption on a close-proximity pair that involves the product of two IPM wave functions $\psi_\alpha(\vec{R}_{12}+\frac{\vec{r}_{12}}{2})$ and $\psi_\beta(\vec{R}_{12}-\frac{\vec{r}_{12}}{2})$ and a two-body operator $\widehat{O}^{[2]}(\vec{R}_{12},\vec{r}_{12})$ (left panel of Fig. 2) is written as a product of a one-body operator $\widehat{O}^{[1]}$ evaluated at the c.m. coordinate $\vec{R}_{12}$ and a correlation operator $\widehat{\ell}$ that depends only on the relative coordinate $\vec{r}_{12}$ (right panel of Fig. 2). In nuclei, $\widehat{\ell}$ has a complicated spin and isospin structure. The ZRA acts as a projection operator on the short-range components of the wave function corresponding with the relative motion of the pair. Throughout this paper the factorized cross section of Eq. (3) is used. The validity of this expression (3) has been experimentally verified. The proposed factorization of the cross section in terms of $F_A^{pp,D}$ was first confirmed in ^{12}C$(e,e'pp)$ measurements back in the late 1990s [9]. An effort is on its way to extract the width of the $F_A^{pp,D}$ distribution in $A(e,e'pp)$ measurements on ^{12}C, ^{27}Al, ^{56}Fe and ^{208}Pb [25, 26], and compare them with the theoretical predictions [22]. Another striking prediction of the expression (3) is that the $A(e,e'pN)$ cross section is proportional to the number of close-proximity pN pairs in the target nucleus. As a result, it can be inferred that the A dependence of the $A(e,e'pp)$ cross section is much softer than naive FSI-corrected $Z(Z-1)/2$ counting. Recent measurements of the $A(e,e'pp)/^{12}$C$(e,e'pp)$ ratios are completely in line with those predictions [27]. The measured and predicted ^{208}Pb/^{12}C $(e,e'pp)$ cross section ratio, for example, is a mere five whereas the naive prediction is over two hundred.

B. Final-state interactions

We include two FSI mechanisms in our model. First, attenuation (ATT) of the outgoing nucleons upon traversing the recoiling nucleus. Second, single-charge exchange (SCX), i.e. an outgoing proton (neutron) rescattering into a neutron (proton). The attenuation effect is calculated in the relativistic multiple-scattering Glauber approximation (RMSGA) [28, 29]. The RMSGA is based on high-energy diffractive scattering. It uses an eikonal form for the

rescattering amplitude dominated by the central term, neglecting spin-dependent attenuation. The RMSGA is fully parameterized in terms of nucleon-nucleon scattering data. We systematically use "FSI" upon referring to the combined effect of attenuation and single-charge exchange. Throughout this paper, we refer to $A(e,e'pN)$ results that ignore the effect of FSI as "ZRA" results.

The distorted c.m. momentum distribution $F_A^{pN,D}(\vec{P}_{12})$ in Eq. (3) is defined in the following way

$$F_A^{pN,D}(\vec{P}_{12}) = \sum_{\alpha,\beta} F_A^{pN,D;\alpha\beta}(\vec{P}_{12}) = \sum_{\substack{s_1,s_2\\ \alpha\beta}} \left| \int d\vec{R}_{12}\, e^{i\vec{P}_{12}\cdot\vec{R}_{12}} \bar{u}(\vec{k}_1,s_1)\psi_\alpha(\vec{R}_{12})\bar{u}(\vec{k}_2,s_2)\psi_\beta(\vec{R}_{12})\mathcal{F}_{\rm RMSGA}(\vec{R}_{12}) \right|^2 . \quad (5)$$

Here, $u(\vec{k},s)$ is the positive-energy free Dirac spinor and (ψ_α, ψ_β) are relativistic mean-field wave functions with IPM quantum numbers (α,β) computed in the Serot-Walecka model [30]. The contribution from a specific IPM nucleon pair with quantum numbers (α,β) is denoted as $F_A^{pN,D;\alpha\beta}(\vec{P}_{12})$. We consider experimental conditions whereby the precise state of the residual $A-2$ nucleus is not resolved. As a result, the sum over (α,β) extends over all occupied pN pairs. In the practical implementation of Eq. (5), we neglect the projection on the lower components of the plane-wave Dirac spinors. The rescattering of the ejected pair with the remaining $A-2$ spectators, encoded in the standard Glauber phase $\mathcal{F}_{\rm RMSGA}$, is computed in the RMSGA [28]. The interactions among the two ejected nucleons do not affect $F_A^{pN,D}(\vec{P}_{12})$ due to c.m. momentum conservation, and they are effectively included in $\sigma_{epN}(\vec{k}_{12})$. The implementation of reinteractions between the ejected nucleons is not addressed in this article, as $\sigma_{epN}(\vec{k}_{12})$ drops out in the cross section ratios defined in Sec. II C.

The SCX mechanisms are treated in a semi-classical manner. The joint probability for the struck proton, labelled "1", undergoing SCX while the recoiling nucleon of the SRC pair, labelled "2", is not undergoing any SCX, is given by

$$P_{\rm CX,A}^{[\mathbf{1}]2,pN} = \sum_{\alpha,\beta} \frac{\int {\rm d}^3\vec{R}_{12}\, P_{\rm CX}^{[\boldsymbol{\alpha}]\beta}(\vec{R}_{12}) \left[1 - P_{\rm CX}^{\alpha[\boldsymbol{\beta}]}(\vec{R}_{12})\right] F_A^{pN,D;\alpha\beta}(\vec{R}_{12})}{\int {\rm d}^3\vec{R}_{12}\, F_A^{pN,D;\alpha\beta}(\vec{R}_{12})} . \quad (6)$$

As in Eq. (5), the sum over (α,β) extends over all the occupied pN pairs. Further, the square bracket [**1**] identifies the nucleon subject to SCX. In Eq. (6), the probability that an initial nucleon with quantum numbers α (with correlated partner with quantum numbers β) has undergone a SCX after a hard interaction at c.m. coordinate $\vec{R}_{12}$ is given by $P_{\rm CX}^{[\boldsymbol{\alpha}]\beta}(\vec{R}_{12})$, and is weighted with the RMSGA-corrected probability $F_A^{pN,D;\alpha\beta}(\vec{R}_{12})$ of finding the two nucleons at c.m. coordinate $\vec{R}_{12}$. Similar expressions to Eq. (6) can be written for the situations where only the recoil nucleon "2" is subject to SCX ($P_{\rm CX,A}^{1[\mathbf{2}],pN}$), both nucleons in the pair are subject to SCX ($P_{\rm CX,A}^{[\mathbf{12}],pN}$) or none of the nucleons in the pair are subject to SCX ($P_{\rm CX,A}^{12,pN}$). In those situations, the factor $P_{\rm CX}^{[\boldsymbol{\alpha}]\beta}(\vec{R}_{12})\left[1 - P_{\rm CX}^{\alpha[\boldsymbol{\beta}]}(\vec{R}_{12})\right]$ in the numerator of Eq. (6), is replaced by respectively the factor $\left[1 - P_{\rm CX}^{[\boldsymbol{\alpha}]\beta}(\vec{R}_{12})\right] P_{\rm CX}^{\alpha[\boldsymbol{\beta}]}(R_{12})$, $P_{\rm CX}^{[\boldsymbol{\alpha}]\beta}(\vec{R}_{12}) P_{\rm CX}^{\alpha[\boldsymbol{\beta}]}(R_{12})$, and $[1 - P_{\rm CX}^{[\boldsymbol{\alpha}]\beta}(\vec{R}_{12})][1 - P_{\rm CX}^{\alpha[\boldsymbol{\beta}]}(\vec{R}_{12})]$. One has $P_{\rm CX,A}^{[\mathbf{1}]2,pN} + P_{\rm CX,A}^{1[\mathbf{2}],pN} + P_{\rm CX,A}^{[\mathbf{12}],pN} + P_{\rm CX,A}^{12,pN} = 1$.

The SCX probabilities $P_{\rm CX}^{[\boldsymbol{\alpha}]\beta}(\vec{R}_{12})$ are calculated in a semi-classical approximation. Thereby, the probability of charge-exchange rescattering for a nucleon with bound-state IPM quantum numbers α that is brought in a continuum state at the coordinate $\vec{r}$ is modelled by

$$P_{\rm CX}^{[\boldsymbol{\alpha}]\beta}(\vec{r}) = 1 - \exp\left[-\sigma_{\rm CX}(s) \int_z^{+\infty} {\rm d}z' \rho_{A-2}^{\alpha\beta}(z')\right] . \quad (7)$$

The z-axis is chosen along the direction of propagation of the nucleon undergoing SCX ($[\boldsymbol{\alpha}]$). The $\rho_{A-2}^{\alpha\beta}$ is the one-body density of the recoiling $A-2$ nucleus that contributes to the SCX reaction. For an ejected proton (neutron)

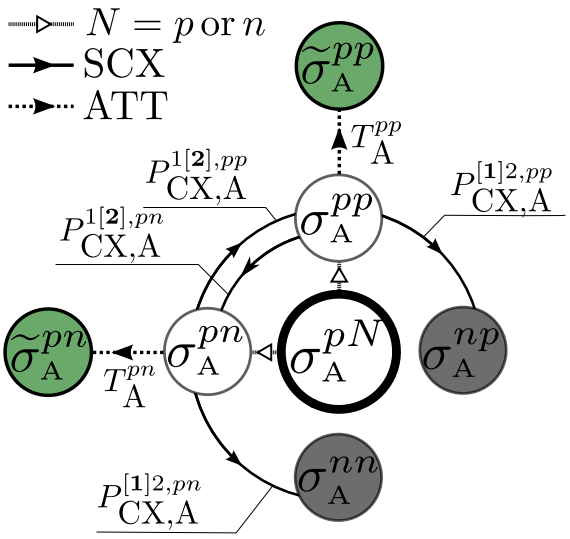

FIG. 3. (Color online) A flow diagram illustrating the different FSI effects included in our model calculations. The center of the diagram ($\sigma_{\rm A}^{pN}$) denotes the plane-wave ZRA $A(e,e'pN)$ cross section. The $\widetilde{\sigma}_{\rm A}^{pp}$ and $\widetilde{\sigma}_{\rm A}^{pn}$ correspond with the observed $A(e,e'pp)$ and $A(e,e'pn)$ cross sections. The solid arrows denote SCX reactions. The dashed arrows denote the attenuation (ATT).

only the neutron (proton) density of the recoiling nucleus affects SCX reactions. The parameter $\sigma_{\rm CX}(s)$ in Eq. (7) can be extracted from elastic proton-neutron scattering data [31], with s the total c.m. energy squared of the two nucleons involved in the SCX. In Ref. [32], it was shown that $\sigma_{\rm CX}(s)$ obeys the relation

$$\sigma_{\rm CX}(s) = 0.424 \frac{s}{s_{800}}\ {\rm fm}^2\,, \tag{8}$$

where s_{800} is the c.m. energy squared for a collision between a neutron with 800 MeV kinetic energy and a stationary proton. The value 0.424 fm^2 is obtained by integrating the elastic pn differential cross section with s=s_{800} at backward scattering angles dominated by charge-exchange [31]. The parameterization of Eq. (8) is valid for lab frame momenta in the interval $[0.1, 100]$ GeV/c.

In Eq. (6), the weight factor $F_{\rm A}^{pN,D;\alpha\beta}(\vec{R}_{12})$ gives the attenuation corrected probability to find a pair (α,β) at a coordinate $\vec{R}_{12}$

$$F_A^{pN,D;\alpha\beta}(\vec{R}_{12}) = \lim_{\vec{r}_{12}\to\vec{0}} |\psi_\alpha(\vec{R}_{12}+\frac{\vec{r}_{12}}{2})|^2 |\psi_\beta(\vec{R}_{12}-\frac{\vec{r}_{12}}{2})|^2 |\mathcal{F}_{\rm RMSGA}(\vec{R}_{12}\pm\frac{\vec{r}_{12}}{2})|^2\,. \tag{9}$$

Note that $F_A^{pN,D;\alpha\beta}(\vec{R}_{12})$ is the Fourier transform of $F_A^{pN,D;\alpha\beta}(\vec{P}_{12})$ appearing in Eq. (3). In the limit of vanishing FSI ($\mathcal{F}_{\rm RMSGA}\equiv 1$) Eq. (9) reduces to the probability of finding two IPM nucleons at the same coordinate $\vec{R}_{12}$.

The flow diagram in Fig. 3 shows an overview of the different FSI mechanisms that are included in the $A(e,e'pN)$ reactions considered in this article. The initial plane-wave (vanishing FSI) ZRA $A(e,e'pN)$ cross section (σ_A^{pN}) is positioned at the center. The partner nucleon can be a proton (σ_A^{pp}) or a neutron (σ_A^{pn}). The observable cross sections are denoted with $\widetilde{\sigma}_A^{pp}$ and $\widetilde{\sigma}_A^{pn}$. The sources and sinks between the different $\widetilde{\sigma}_A^{NN}$ through the SCX mechanism are denoted with the solid arrows. The dashed arrows denote the RMSGA attenuation contribution, quantified by means

of the nuclear transparency T_A^{pN}, defined as the ratio of the $A(e,e'pN)$ cross section with and without the RMSGA attenuations (see Eq. (14)). It is a measure for attenuation caused by the nuclear medium. The different contributions to the final cross sections $\widetilde{\sigma}_A^{pp}$, $\widetilde{\sigma}_A^{pn}$ can be visually deduced by following all possible paths from σ_A^{pN} to $\widetilde{\sigma}_A^{pp}$ or $\widetilde{\sigma}_A^{pn}$ in Fig. (3). Because we only account for single-charge exchange, the SCX arrows can only be used at most once for each particle in every path, meaning $P_{\mathrm{CX,A}}^{\mathbf{1}[\mathbf{2}],pN} P_{\mathrm{CX,A}}^{[\mathbf{1}]\mathbf{2},pN}$ is allowed but $P_{\mathrm{CX,A}}^{[\mathbf{1}]\mathbf{2},pN} P_{\mathrm{CX,A}}^{[\mathbf{1}]\mathbf{2},pN}$ or $P_{\mathrm{CX,A}}^{\mathbf{1}[\mathbf{2}],pN} P_{\mathrm{CX,A}}^{\mathbf{1}[\mathbf{2}],pN}$ are not. The missing SCX arrows (from and between σ_A^{nn}, σ_A^{np}) are neglected as we assume that the struck nucleon is a proton. We argue that this is a valid approximation. First, the photon-neutron coupling is a fraction of the photon-proton one. Second, an SCX reaction is a necessary condition to end up with a leading proton in the final state. We find that those SCX probabilities are very small (Sec. III).

C. $A(e,e'pN)$ cross-section ratios

Most often, it is extremely challenging to measure $A(e,e'pN)$ cross sections. A lot of information regarding nuclear SRC has been obtained by measuring cross-section rations over extended ranges of the phase space [4, 5, 21, 25, 27]. Using the factorized form of the differential cross section from Eq. (3), one can investigate $A(e,e'pN)$ cross-section ratios relative to ^{12}C. Let $\widetilde{R}_A^{pN}$ (R_A^{pN}) be the cross-section ratios with (without) the inclusion of FSI,

$$\widetilde{R}_A^{pN} = \frac{\widetilde{\sigma}_A^{pN}}{\widetilde{\sigma}_{^{12}\mathrm{C}}^{pN}} \approx \frac{\int \mathrm{d}^2\Omega_{k_{e'}} \mathrm{d}^3\vec{k}_{12}\sigma_{epN}(\vec{k}_{12}) \int \mathrm{d}^3\vec{P}_{12} F_A^{pN,D}(\vec{P}_{12})}{\int \mathrm{d}^2\Omega_{k_{e'}} \mathrm{d}^3\vec{k}_{12}\sigma_{epN}(\vec{k}_{12}) \int \mathrm{d}^3\vec{P}_{12} F_{^{12}\mathrm{C}}^{pN,D}(\vec{P}_{12})} = \frac{\int \mathrm{d}^3\vec{P}_{12} F_A^{pN,D}(\vec{P}_{12})}{\int \mathrm{d}^3\vec{P}_{12} F_{^{12}\mathrm{C}}^{pN,D}(\vec{P}_{12})}\,. \tag{10}$$

The $\widetilde{\sigma}_A^{pN}$ denotes the FSI-corrected $A(e,e'pN)$ cross section. The cross-section ratios are independent of the information contained in the photon-nucleon coupling $\sigma_{epN}(\vec{k}_{12})$. Therefore, we use cross-section ratios to quantify the effect of SRC as those are less model dependent.

In the limit of vanishing FSI the integrated c.m. momentum distribution $\int \mathrm{d}^3\vec{P}_{12}\, F_A^{pN,D}(\vec{P}_{12})$ is proportional to the amount of SRC-susceptible pN pairs. The relative amount of SRC pairs for nucleus A relative to ^{12}C is then given by $R_{pN} = \sigma_A^{pN}/\sigma_{^{12}\mathrm{C}}^{pN}$, where σ_A^{pN} denotes the $A(e,e'pN)$ cross section in the limit of vanishing FSI. It is well established that the tensor correlation [3, 19] induces a heavy dominance of SRC pn pairs over SRC pp pairs. This dominance is not automatically generated in the ZRA without introducing additional assumptions with regard to the dynamical mechanisms underlying the SRC. The pn- over pp-pair dominance can be included for nucleus A using the measured pn/pp pair ratio (18 ± 5) in ^{12}C [19], in the following way

$$\frac{\sigma_A^{pn}}{\sigma_A^{pp}} = \frac{\sigma_A^{pn}}{\sigma_{^{12}\mathrm{C}}^{pn}} \frac{\sigma_{^{12}\mathrm{C}}^{pn}}{\sigma_{^{12}\mathrm{C}}^{pp}} \frac{\sigma_{^{12}\mathrm{C}}^{pp}}{\sigma_A^{pp}} \approx \frac{\sigma_A^{pn}}{\sigma_{^{12}\mathrm{C}}^{pn}} \frac{\#pn\text{-pairs}\,(^{12}\mathrm{C})}{2\cdot\#pp\text{-pairs}\,(^{12}\mathrm{C})} \frac{\sigma_{^{12}\mathrm{C}}^{pp}}{\sigma_A^{pp}} \approx \frac{\sigma_A^{pn}}{\sigma_{^{12}\mathrm{C}}^{pn}} \left(\frac{18\pm5}{2}\right) \frac{\sigma_{^{12}\mathrm{C}}^{pp}}{\sigma_A^{pp}}\,. \tag{11}$$

The exchanged photon can couple to both protons in a pp pair and to one in a pn pair leading to the factor 2 in the denominator of Eq. (11). The expressions for the FSI-corrected cross-section ratios, $\widetilde{R}^{pN} = \widetilde{\sigma}_A^{pN}/\widetilde{\sigma}_{^{12}\mathrm{C}}^{pN}$, are then given by (see Fig. 3)

$$\begin{aligned}\widetilde{R}_A^{pp} = \frac{\widetilde{\sigma}_A^{pp}}{\widetilde{\sigma}_{^{12}\mathrm{C}}^{pp}} &= \frac{P_{\mathrm{CX,A}}^{12,pp} T_A^{pp} \sigma_A^{pp} + P_{\mathrm{CX,A}}^{\mathbf{1}[\mathbf{2}],pn} T_A^{p*} \sigma_A^{pn}}{P_{\mathrm{CX}^{12}\mathrm{C}}^{12,pp} T_{^{12}\mathrm{C}}^{pp} \sigma_{^{12}\mathrm{C}}^{pp} + P_{\mathrm{CX}^{12}\mathrm{C}}^{\mathbf{1}[\mathbf{2}],pn} T_{^{12}\mathrm{C}}^{p*} \sigma_{^{12}\mathrm{C}}^{pn}} = \frac{P_{\mathrm{CX,A}}^{12,pp} T_A^{pp} R_A^{pp} + P_{\mathrm{CX,A}}^{\mathbf{1}[\mathbf{2}],pn} T_A^{p*} \frac{\sigma_A^{pn}}{\sigma_{^{12}\mathrm{C}}^{pp}}}{P_{\mathrm{CX}^{12}\mathrm{C}}^{12,pp} T_{^{12}\mathrm{C}}^{pp} + P_{\mathrm{CX}^{12}\mathrm{C}}^{\mathbf{1}[\mathbf{2}],pn} T_{^{12}\mathrm{C}}^{p*} \frac{\sigma_{^{12}\mathrm{C}}^{pn}}{\sigma_{^{12}\mathrm{C}}^{pp}}} \\ &= \frac{P_{\mathrm{CX,A}}^{12,pp} T_A^{pp} R_A^{pp} + P_{\mathrm{CX,A}}^{\mathbf{1}[\mathbf{2}],pn} T_A^{p*} R_A^{pn} \frac{18\pm5}{2}}{P_{\mathrm{CX}^{12}\mathrm{C}}^{12,pp} T_{^{12}\mathrm{C}}^{pp} + P_{\mathrm{CX}^{12}\mathrm{C}}^{\mathbf{1}[\mathbf{2}],pn} T_{^{12}\mathrm{C}}^{p*} \frac{18\pm5}{2}}\,.\end{aligned} \tag{12}$$

Here, $\widetilde{\sigma}_A^{pN}$ is the FSI corrected $A(e,e'pN)$ cross section. The first term in the numerator and denominator consists of the $A(e,e'pp)$ cross section (σ_A^{pp}) corrected for attenuation (T_A^{pp}) given that no SCX occurred ($P_{\rm CX,A}^{12,pp}$). The second term is the contribution from an initial $A(e,e'pn)$ (σ_A^{pn}) multiplied by the attenuation factor (T_A^{p*}) given that the recoiling partner changes to a proton ($P_{\rm CX,A}^{1[\mathbf{2}],pn}$). These two terms correspond with the two possible paths to $\widetilde{\sigma}_A^{pp}$ in Fig. 3 :

$$\sigma_A^{pN} \rightarrow \sigma_A^{pp} \xrightarrow{P_{\rm CX,A}^{12,pp} T_A^{pp}} \widetilde{\sigma}_A^{pp} \quad \text{and,} \quad \sigma_A^{pN} \rightarrow \sigma_A^{pn} \xrightarrow{P_{\rm CX,A}^{1[\mathbf{2}],pn} T_A^{p*}} \widetilde{\sigma}_A^{pp} \, . \tag{13}$$

In the ZRA, the nuclear $A(e,e'pN)$ transparency T_A^{pN} can be calculated as,

$$T_A^{pN} \approx \frac{\int \mathrm{d}^3\vec{P}_{12}\, F_A^{pN,D}(\vec{P}_{12})}{\int \mathrm{d}^3\vec{P}_{12}\, F_A^{pN}(\vec{P}_{12})} \, . \tag{14}$$

Here, $F_A^{pN}(\vec{P}_{12})$ is the c.m. momentum distribution in the limit of vanishing attenuation ($\mathcal{F}_{\rm RMSGA} \equiv 1$ in Eq. (5)). We stress that the transparency depends on the sampled phase space, i.e. the integration volume of $\vec{P}_{12}$ in Eq. (14).

In estimating the attenuation effect for the SCX contribution we use the averaged transparency $T_A^{p*} = \frac{1}{2}(T_A^{pp} + T_A^{pn})$. The reason is that in our model we have no information about the time ordering of the SCX and attenuation mechanisms. Therefore, starting from initial pp knockout followed by $p \rightarrow n$ SCX, one can adopt the averaged attenuation $\frac{T_A^{pn}+T_A^{pp}}{2}$. Note that the difference between T_A^{pp} and T_A^{pn} is rather small for the kinematics addressed in this paper (2% for ^{12}C and about 20% for ^{208}Pb).

For the $A(e,e'pn)$ cross-section ratios we get,

$$\widetilde{R}_A^{pn} = \frac{\widetilde{\sigma}_A^{pn}}{\widetilde{\sigma}_{^{12}\mathrm{C}}^{pn}} = \frac{P_{\rm CX,A}^{12,pn} T_A^{pn} \sigma_A^{pn} + P_{\rm CX,A}^{1[\mathbf{2}],pp} T_A^{p*} \sigma_A^{pp}}{P_{\rm CX^{12}C}^{12,pn} T_{^{12}\mathrm{C}}^{pn} \sigma_{^{12}\mathrm{C}}^{pn} + P_{\rm CX^{12}C}^{1[\mathbf{2}],pp} T_{^{12}\mathrm{C}}^{p*} \sigma_{^{12}\mathrm{C}}^{pp}} = \frac{P_{\rm CX,A}^{12,pn} T_A^{pn} R_A^{pn} + P_{\rm CX,A}^{1[\mathbf{2}],pp} T_A^{p*} R_A^{pp} \frac{2}{18\pm5}}{P_{\rm CX^{12}C}^{12,pn} T_{^{12}\mathrm{C}}^{pn} + P_{\rm CX^{12}C}^{1[\mathbf{2}],pp} T_{^{12}\mathrm{C}}^{p*} \frac{2}{18\pm5}} \, . \tag{15}$$

As in Eq. (12) each term can be identified with a certain path to $\widetilde{\sigma}_A^{pn}$ in Fig. 3. The experimental values for $\widetilde{R}_A^{pn}$ are not known if the outgoing neutrons are not detected. In kinematics tuned so that the $A(e,e'p)$ signal is dominated by $A(e,e'pN)$ events it is possible to deduce $\widetilde{R}_A^{pn}$ from the $A(e,e'p)$ cross section ratios ($\widetilde{R}_A^{p}$) measured for the same kinematical settings

$$\widetilde{R}_A^{p} = \frac{\widetilde{\sigma}_A^{p}}{\widetilde{\sigma}_{^{12}\mathrm{C}}^{p}} \approx \frac{2\widetilde{\sigma}_A^{pp} + \widetilde{\sigma}_A^{pn}}{2\widetilde{\sigma}_{^{12}\mathrm{C}}^{pp} + \widetilde{\sigma}_{^{12}\mathrm{C}}^{pn}} = \frac{2\widetilde{R}_A^{pp} + \widetilde{R}_A^{pn} \widetilde{R}_{^{12}\mathrm{C}}^{\frac{pn}{pp}}}{2 + \widetilde{R}_{^{12}\mathrm{C}}^{\frac{pn}{pp}}} \, . \tag{16}$$

The $^{12}\mathrm{C}(e,e'pn)$ over $^{12}\mathrm{C}(e,e'pp)$ cross-section ratio $\widetilde{R}_{^{12}\mathrm{C}}^{\frac{pn}{pp}}$ can be extracted in the following way

$$\widetilde{R}_{^{12}\mathrm{C}}^{\frac{pn}{pp}} = \frac{\widetilde{\sigma}_{^{12}\mathrm{C}}^{pn}}{\widetilde{\sigma}_{^{12}\mathrm{C}}^{pp}} = \frac{P_{\rm CX^{12}C}^{12,pn} T_{^{12}\mathrm{C}}^{pn} \sigma_{^{12}\mathrm{C}}^{pn} + P_{\rm CX^{12}C}^{1[\mathbf{2}],pp} T_{^{12}\mathrm{C}}^{p*} \sigma_{^{12}\mathrm{C}}^{pp}}{P_{\rm CX^{12}C}^{12,pp} T_{^{12}\mathrm{C}}^{pp} \sigma_{^{12}\mathrm{C}}^{pp} + P_{\rm CX^{12}C}^{1[\mathbf{2}],pn} T_{^{12}\mathrm{C}}^{p*} \sigma_{^{12}\mathrm{C}}^{pn}} = \frac{P_{\rm CX^{12}C}^{12,pn} T_{^{12}\mathrm{C}}^{pn} \frac{18\pm5}{2} + P_{\rm CX^{12}C}^{1[\mathbf{2}],pp} T_{^{12}\mathrm{C}}^{p*}}{P_{\rm CX^{12}C}^{12,pp} T_{^{12}\mathrm{C}}^{pp} + P_{\rm CX^{12}C}^{1[\mathbf{2}],pn} T_{^{12}\mathrm{C}}^{p*} \frac{18\pm5}{2}} \, . \tag{17}$$

Hence from Eq. (16),

$$\widetilde{R}_A^{pn} = \frac{1}{\widetilde{R}_{^{12}\mathrm{C}}^{\frac{pn}{pp}}} \left[\widetilde{R}_A^{p} \left(2 + \widetilde{R}_{^{12}\mathrm{C}}^{\frac{pn}{pp}} \right) - 2\widetilde{R}_A^{pp} \right] \, . \tag{18}$$

The relations for $\widetilde{R}_A^{pp}$ and $\widetilde{R}_A^{pn}$ can be inverted to extract the FSI-uncorrected cross section ratios (which are proportional to the ratios of SRC prone pairs) R_A^{pp}, R_A^{pn} from the measured values for $\widetilde{R}^{pp}$ and $\widetilde{R}^{pn}$ [27].

III. RESULTS

In this section we present the results of the numerical $A(e,e'pN)$ calculations for four representative target nuclei and two representative but distinct kinematic settings. First, we apply the formalism developed in the previous section to the $A(e,e'pN)$ reaction in the kinematics covered by the Jefferson Lab CLAS detector [21]. The latter is a "4π" detector, which results in a very large phase-space coverage. We systematically refer to this kinematics as "KinB". Kinematics approaching a "4π" layout pose challenges for the calculations and require dedicated sampling techniques that are outlined below. After the discussion of the "4π" KinB results we present two-nucleon knockout calculations in kinematics in very narrow solid angles for all detected particles (coined "KinA").

In dealing with the KinB situation, we define a reference frame with the z-axis along the initial momentum $\vec{k}_1$ of the proton and the exchanged photon-momentum $\vec{q}$ in the $x-z$ plane. A two-nucleon knockout event is uniquely characterized by the set of 6 kinematical variables $\{Q^2 \equiv |\vec{q}|^2 - \omega^2, x_B = \frac{Q^2}{2m_N\omega}, \theta_q, \vec{P}_{12}\}$. Here, θ_q is the direction of $\vec{q}$ relative to the z axis.

Upon numerically computing the distorted c.m. momentum distribution of Eq. (5), we generate phase space samples by drawing (x_B,Q^2) from the experimentally measured (x_B, Q^2) distribution [25]. We draw the θ_q and the $\vec{P}_{12}$ uniformly from the relevant ranges. In order to guarantee that the virtual photon primarily probes correlated pairs a number of kinematic constraints are imposed

$$\theta_{\vec{p}_1,\vec{q}} \leq 25^\circ \; ; \; 0.62 < \frac{|\vec{p}_1|}{|\vec{q}|} < 0.96 \; ; \; x_B \geq 1.2; \tag{19}$$

$$|\vec{k}_1| \geq 300 \text{ MeV}; |\vec{p}_2| \geq 350 \text{ MeV}\,. \tag{20}$$

The first two cuts select events where the virtual photon has mainly interacted with the struck (leading) proton. The $x_B \geq 1.2$ cut selects events with a high $|\vec{q}|$ and relatively low ω, suppressing for example pion production through intermediate Δ production. The last two cuts impose high-momentum conditions (larger than the Fermi momentum) for the initial nucleon pair.

Sampling over the complete $\{x_B$,Q^2,θ_q,$\vec{P}_{12}\}$ space is computationally very demanding in the RMSGA calculations. Therefore, we use stratified sampling on the binned plane-wave result $F_A^{pN}(\vec{P}_{12}) = F_A^{pN,D}(\vec{P}_{12}|\mathcal{F}_{\text{RMSGA}} \equiv 1)$, to generate the events in phase space (see Fig. 4 for an illustration). Thereby, after calculating $F_A^{pN}(\vec{P}_{12})$ for a large number of events, we bin the events in the $\vec{P}_{12}$ space. Next, we sample phase-space events from the bins using the bin-averaged value $\overline{F}_A^{pN}(\vec{P}_{12})$ of $F_A^{pN}(\vec{P}_{12})$ as bin weights. We then include the effect of attenuation by calculating $F_A^{pN,D}(\vec{P}_{12})$ in the RMSGA, for the sampled phase-space events. It is assumed that the bin averaged $\overline{F}_A^{pN,D}(\vec{P}_{12})$ of the function $F_A^{pN,D}(\vec{P}_{12})$ of the sampled events is representative for the real bin average. Using this procedure, the integrals in Eq. (10) are determined in the following way:

$$\int \mathrm{d}^3\vec{P}_{12} F_A^{pN,D}(\vec{P}_{12}) \approx \frac{V_{\vec{P}_{12}}}{N_s} \sum_{n\in\text{bins}} \overline{F}_{A,n}^{pN,D}(\vec{P}_{12}) N_n\,, \tag{21}$$

with N_n the number of events in the n-th bin, N_s the total number of phase-space events and $V_{\vec{P}_{12}}$ the considered phase-space volume in $\vec{P}_{12}$.

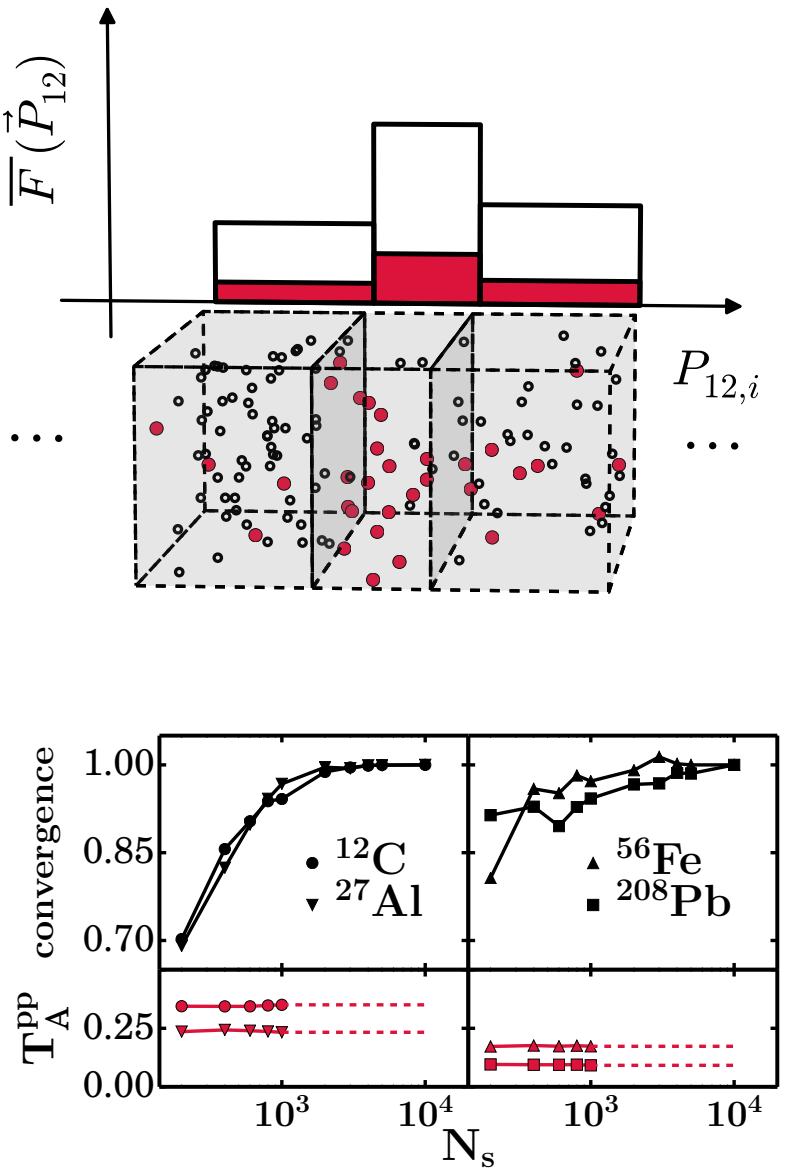

FIG. 4. (Color online) (Top) A schematic representation of the sampling procedure adopted in the $A(e,e'pN)$ calculations in kinematics covering a large phase space. The gray cubes are $\vec{P}_{12}$ bins. The black circles are those points in $\vec{P}_{12}$ space for which $A(e,e'pN)$ calculations with vanishing FSI ($\mathcal{F}_{\rm RMSGA} \equiv 1$) are done. The red dots represent the sampled points for which the RMSGA $A(e,e'pN)$ calculations are performed. The sampling weight of each bin is the bin-averaged c.m. momentum distribution $\overline{F}_A^{pN}(\vec{P}_{12})$ indicated by the white bars. The resulting bin-averaged c.m. momentum distribution including FSI is indicated by the red bars. (Bottom) The convergence as defined in Eq. (22) and the transparency T_A^{pp} of Eq. (14) as a function of the sample size N_s for $(e,e'pp)$ from ^{12}C, ^{27}Al, ^{56}Fe and ^{208}Pb in the kinematics defined by Eq. (20).

Fig. 4 displays the convergence of the plane-wave integrated c.m. distribution, defined as,

$$\frac{\left[\int \mathrm{d}^3\vec{P}_{12} F_A^{pN}(\vec{P}_{12})\right]_{N_s}}{\left[\int \mathrm{d}^3\vec{P}_{12} F_A^{pN}(\vec{P}_{12})\right]_{N_s=10^4}}, \tag{22}$$

and the nuclear transparency T_A^{pp} (Eq. (14)) as a function of the number of sampled events N_s. The convergence at a

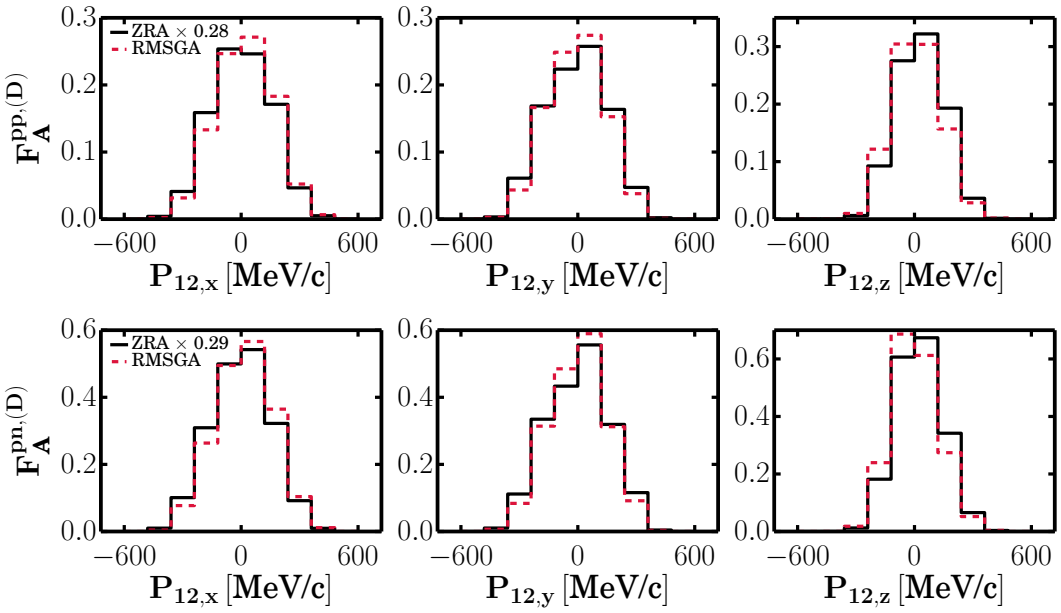

FIG. 5. (Color online) The $P_{12,x}$,$P_{12,y}$,$P_{12,z}$ dependence of the c.m. momentum distribution $F_A^{pN}(\vec{P}_{12})$ (ZRA in the plane-wave limit of the ejected nucleons) and $F_A^{pN,D}(\vec{P}_{12})$ (including elastic attenuation of the ejected nucleons) for ^{12}C$(e,e'pp)$ (top) and ^{12}C$(e,e'pn)$ (bottom) in KinB kinematics. The solid lines, obtained in the ZRA are multiplied with the nuclear transparency for ^{12}C (Table I).

1000 samples is between 94% and 97% for all nuclei. We perform the RMSGA calculations for this sample size. From Fig. 4 it is clear that the nuclear transparency is almost independent of the sample size. This indicates that the ZRA and RMSGA (≡ZRA+RMSGA) have almost identical convergence behavior as a function of the sample size N_s.

Figures 5 and 6 show the computed c.m. distribution for $A(e,e'pp)$ and $A(e,e'pn)$. Both undistorted (ZRA, $F^{pN}(\vec{P}_{12})$) and distorted (RMSGA, $F^{pN,D}(\vec{P}_{12})$) results are shown. It is clear that for all target nuclei considered, attenuation effects on the ejected nucleons marginally affect the shape of the c.m. momentum distribution. Note that the shape of the c.m. momentum distribution is fairly similar for all four nuclei considered. This illustrates that SRC are connected with the local and "universal" short-distance behavior of nucleon pairs [3].

The opening angle θ_{12} is defined as the angle between the two initial nucleon momenta, $\cos\theta_{12} = (\vec{k}_1 \cdot \vec{k}_2)/(|\vec{k}_1||\vec{k}_2|)$. Nucleon pairs susceptible to SRC have a high relative momentum and a small c.m momentum, reminiscent of "back-to-back" motion. This causes the opening-angle distribution of SRC pairs to be biased towards backward angles. Figure 7 displays the normalized θ_{12} distributions as they can be extracted from the undistorted and distorted distributions $F^{pN}(\vec{P}_{12})$ and $F^{pN,D}(\vec{P}_{12})$ for the different nuclei. The inclusion of elastic attenuation mechanisms as computed in the RMSGA framework, has a relatively small effect on the opening-angle distribution. A slight tendency to effectively increase the contributions of the $\cos\theta_{12} \approx -1$ events is observed.

Charge-exchange reactions in the final state will mix the c.m. momentum distribution and the opening-angle distribution of the initial pp- and pn-pairs. For example initial pp-pairs, with a c.m. momentum distribution $F_A^{pp,D}(\vec{P}_{12})$, can change into pn-pairs, contaminating $F_A^{pn,D}(\vec{P}_{12})$ and vice versa. From Figs. 5 to 7 it is clear that throughout the mass table the $A(e,e'pp)$ and $A(e,e'pn)$ c.m. momentum distributions as well as the opening angle distributions are very similar. The effect of SCX on the shape of these distributions is close to negligible. The SCX probabilities

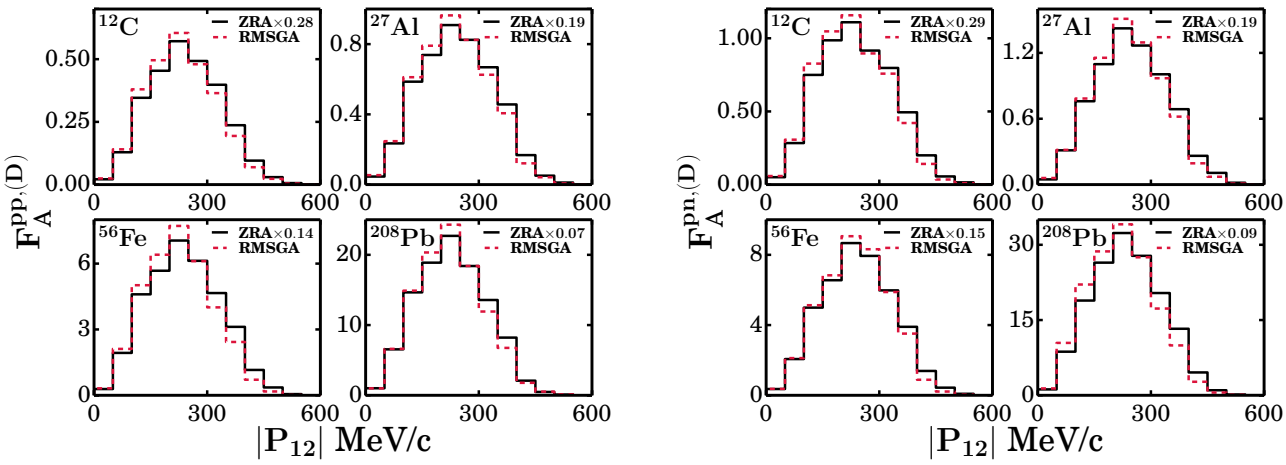

FIG. 6. (Color online) The c.m. momentum distribution in the ZRA $F_A^{pN,(D)}(\vec{P}_{12})$ with and without RMSGA attenuation corrections for $A(e,e'pp)$ (left) and $A(e,e'pn)$ (right) in KinB kinematics. As in Fig. 5 the ZRA results are multiplied with the corresponding T_A^{pN} (see Table I).

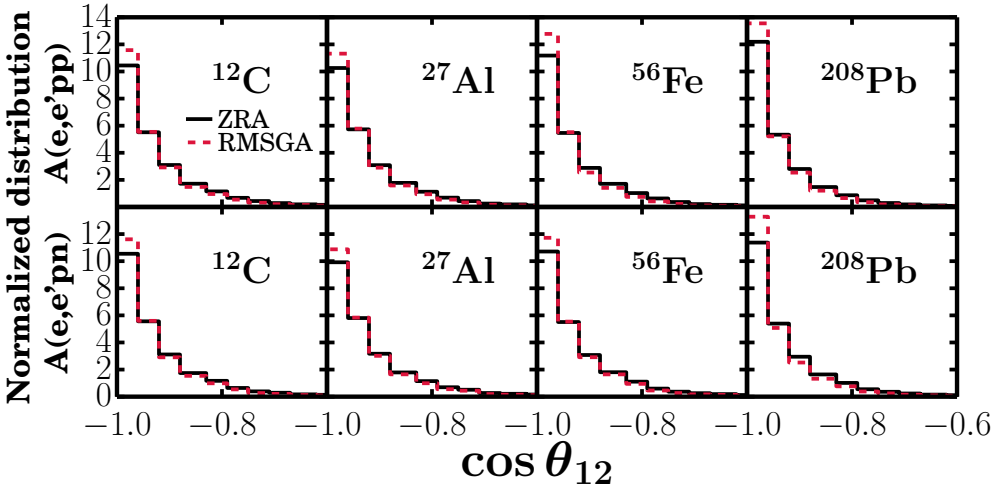

FIG. 7. (Color online) The normalized θ_{12} distributions for $A(e,e'pp)$ (top) and $A(e,e'pn)$ (bottom) in KinB kinematics.

calculated in the ZRA and ZRA+RMSGA (Eq. 6) are displayed in Fig. 8. The RMSGA clearly diminishes the SCX probabilities. This can be understood in the following way: the events most susceptible to SCX reactions are those whereby the ejected nucleon pair traverses large distances in the recoiling nucleus. These events are most suppressed by the attenuation, causing the SCX probabilities to decrease.

Table I lists the cross-section ratios R_A^{pN} calculated in the ZRA. These are approximately equal to the SRC pair ratios. The nuclear transparencies T_A^{pN} calculated in the RMSGA (Eq. (14)) and the FSI (RMSGA+SCX) corrected cross section ratios $\widetilde{R}_A^{pN}$ are listed as well. The RMSGA attenuates the cross sections significantly, ranging from a factor of four for ^{12}C to fourteen for ^{208}Pb. The inclusion of SCX has a very modest effect on the cross section ratios $\widetilde{R}_A^{pN}$, the largest effect is approximately 8% for $\widetilde{R}^{pp}_{^{208}\mathrm{Pb}}$.

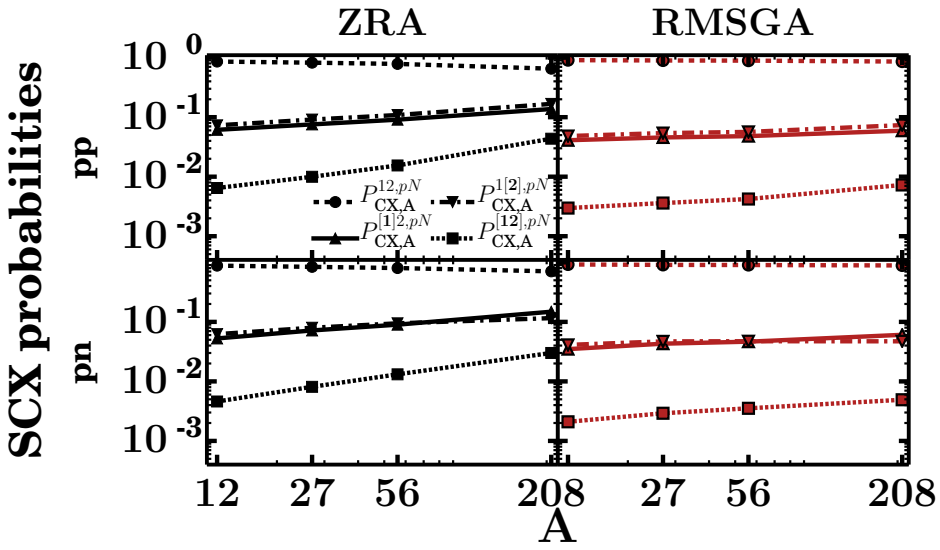

FIG. 8. (Color online) The mass dependence of the SCX probabilities for $A(e,e'pp)$ (top) and $A(e,e'pn)$ (bottom) for KinB. $P^{12,pN}_{\rm CX,A}$ is the probability that no charge exchange scattering occurs. $P^{[\mathbf{1}],2,pN}_{\rm CX,A}$, $P^{1,[\mathbf{2}],pN}_{\rm CX,A}$ are the probabilities that either the leading or the recoil nucleon undergoes charge exchange. $P^{[\mathbf{1},\mathbf{2}],pN}_{\rm CX,A}$ is the probability that both the leading proton and recoiling nucleon undergo charge exchange. The black lines (left) are calculated in the ZRA, the red ones (right) include RMSGA attenuation.

	R_A^{pp}	T_A^{pp}	$\widetilde{R}_A^{pp}$	R_A^{pn}	T_A^{pn}	$\widetilde{R}_A^{pn}$	$(T_A^p)^2$
^{12}C	1.00	0.280	1.00	1.00	0.286	1.00	0.26
^{27}Al	2.89	0.186	$1.91^{+0.01}_{-0.01}$	2.52	0.186	$1.65^{+0.01}_{-0.01}$	–
^{56}Fe	5.89	0.138	$2.85^{+0.01}_{-0.01}$	4.82	0.150	$2.49^{+0.01}_{-0.01}$	0.10
^{208}Pb	17.44	0.073	$4.96^{+0.11}_{-0.14}$	18.80	0.093	$6.00^{+0.01}_{-0.01}$	0.05

TABLE I. The numerical results for the cross-section ratios R_A^{pN} (ZRA) and the corresponding transparencies (Eq. 14) calculated with the RMSGA. $\widetilde{R}_A^{pN}$ are the cross section ratios corrected for FSI (RMSGA and SCX). For vanishing SCX probabilities $\widetilde{R}_A^{pN}$ is equal to $R_A^{pN}T_A^{pN}/T_{^{12}\rm C}^{pN}$. T_A^p is the measured $A(e,e'p)$ transparency [29].

The mass dependence of the calculated transparencies for the "4π" kinematics KinB follow a power law ($T_A^{pN} \propto A^{\lambda}$) and are displayed in Fig. 9. Up to now we concentrated on the kinematics accessed in the experiment of Ref. [21].

We test the robustness of our methodology by applying it to the kinematics accessed in the ^{12}C$(e,e'pp)$ measurements of Ref. [18], denoted KinA. It corresponds with a very selective phase space whereby the scattered electron and leading proton are detected with two high resolution spectrometers at the fixed central angles 19.5° (electron) and -35.8° (leading proton) relative to the incoming electron beam. The angular acceptance is ±0.03 mrad (±0.06 mrad) in the horizontal (vertical) plane. The initial (final) electron momentum is fixed at 4.627 GeV/c (3.724 GeV/c). The leading proton momentum is $1.42 \pm 4\%$ GeV/c. The recoiling proton is detected at the central angle -99° with an angular acceptance of 96 msr. These kinematics are finely tuned and optimized to select knockout reactions of initial back-to-back pairs. For example, more than 80% of the available phase space has opening angle $\cos\theta_{12} < -0.9$.

The power-law dependencies of the T_A^{pN} transparencies in KinA and KinB kinematics are very similar and are included in Fig. 9. We find $T_A^{pp} \propto A^{-0.46\pm0.02}$ (KinB), $T_A^{pp} \propto A^{-0.49\pm0.06}$ (KinA), $T_A^{pn} \propto A^{-0.38\pm0.03}$ (KinB) and

$T_A^{pn} \propto A^{-0.42\pm0.05}$ (KinA). This indicates that the mass dependence of the transparency is robust. The absolute value of the KinA transparencies is lower by approximately a factor of 2 compared to the KinB results. Given the small phase space of KinA we cannot make a detailed study of the c.m. momentum distribution $F_A^{pN,(D)}$ and the opening-angle distribution, as was done for KinB. Indeed, KinA kinematics only covers restricted ranges in $\vec{P}_{12}$ and $\cos\theta_{12}$.

Next, we outline an alternative method to account for the mass dependence of T_A^{pN}. The transparency T_A^p of $A(e,e'p)$ processes can be interpreted as the probability of a single proton leaving the nucleus after virtual photon excitation. Recent measurements [25] have confirmed that the A dependence of the T_A^p can be captured by the power-law $A^{-0.33}$ [33] . One could naively expect that $T_A^{pp} \approx T_A^p T_A^p \approx A^{-0.66}$. Upon squaring the T_A^p one assumes that the two protons are independent. This is in obvious contradiction with the ZRA picture for SRC-driven two-nucleon knockout reaction where the nucleon pair is maximally correlated: finding one nucleon at the spatial coordinate $\vec{R}_{12}$ fixes the second nucleon's spatial coordinate. To obtain a deeper and more intuitive understanding of the A dependence of T_A^{pN} we have developed a toy model detailed in Appendix A. Thereby the nucleus is treated as a uniform sphere with radius $R = 1.2A^{-\frac{1}{3}}$ fm and density $\rho = \frac{A}{4/3\pi R^3} = 0.138$ fm^{-3}. We calculate the transparencies using a semi-classical approach analogous to the method used to compute the SCX probabilities. The attenuation is derived using the scattering probabilities as in Eq. (7), where the scattering cross section is treated as a model parameter. We derive a range $\lambda \in [-0.37, -0.78]$ for the exponent λ in $T_A^{pN} \propto A^\lambda$. This range is established by varying two parameters: (1) the nucleon-nucleus cross section describing the attenuation, (2) the θ_{12} distribution for the nucleon pair is varied from a uniform distribution (no angular correlation) to a back-to-back delta function $\delta(\theta_{12} - \pi)$. The exponents derived involving the full calculations (Fig. 9) are well in agreement with the toy model. The toy model predicts that for increasingly backward peaked θ_{12} distributions the exponent λ becomes more negative. The toy model also explains why the T_A^{pN} diminishes as one increasingly selects back-to-back nucleons.

IV. SUMMARY

We have studied the impact of final-state interactions in SRC-driven exclusive $A(e,e'pN)$ processes. Attenuation through elastic and soft inelastic rescattering as well as single-charge exchange processes are included in the description of the FSI. We applied our model to two very different kinematics probing SRC pairs and four target nuclei from carbon to lead. It is shown that the inclusion of FSI has a limited effect on the extracted shapes of the c.m. momentum and opening-angle distributions of the correlated nucleon pair. The cross section, however, is significantly attenuated by the FSI. The absolute values of the transparencies depend on the kinematics and we find $T_A^{pN} \approx 0.2 - 0.3$ for a light nucleus like ^{12}C and $T_A^{pN} \approx 0.04 - 0.07$ for a heavy nucleus like ^{208}Pb. The mass dependence of the nuclear transparency is more robust. We find $T_A^{pp} \propto A^{-0.46\pm0.02}$ and $T_A^{pn} \propto A^{-0.38\pm0.03}$ in "4π" kinematics. For the highly selective kinematics, that exclusively probes back-to-back nucleons, we find $T_A^{pp} \propto A^{-0.49\pm0.06}$ and $T_A^{pn} \propto A^{-0.42\pm0.05}$. Both are softer than one would expect from a doubling of the power found for single-nucleon knockout ($T_\mathrm{A}^p \propto A^{-0.33}$). The values for the exponent λ in the power-law dependence of $T_A^{pN} \propto A^\lambda$ are tested against the results of a toy model which allows us to set bounds on values for λ. We find the calculated values to be well within these bounds, $\lambda \in [-0.37, -0.78]$.

It is well known that exclusive $A(e,e'p)$ reactions, populating low-lying states in the residual $(A-1)^*$ nucleus, are

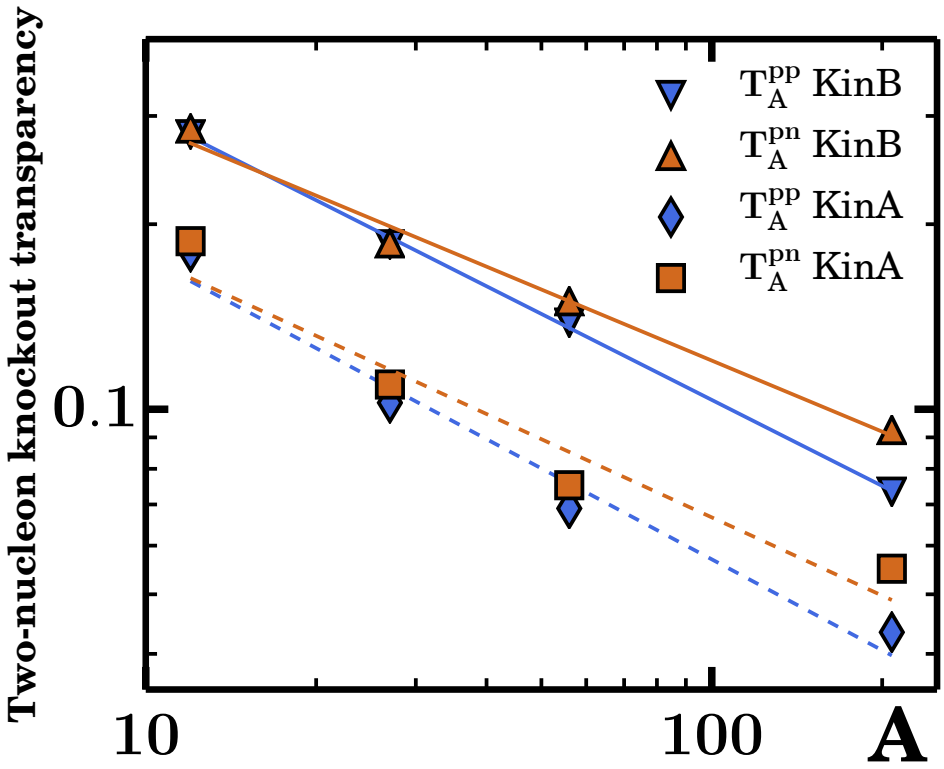

FIG. 9. (Color online) Mass dependence of the two-nucleon knockout transparency calculated according to Eq. (14). The lines are power-law fits ($\sim A^{\lambda}$) to the numerical predictions. KinB denotes the results for the $A(e,e'pN)$ kinematics accessed in Ref. [21] covering a large phase space. KinA are the transparencies calculated for $A(e,e'pN)$ in the kinematics accessed in Ref. [18] with very selective phase space.

proportional to the FSI corrected single-particle momentum distributions for specific hole states. Along similar lines, the SRC-driven $A(e,e'pN)$ cross section is proportional to the c.m. distribution of close-proximity pairs. We find that the FSI only modestly affect the shape of the c.m. distribution, with the width of the distribution barely changing. In essence, to a reasonable degree of accuracy, the aggregated effect of FSI for exclusive $A(e,e'pN)$ processes is a sizeable reduction of the plane-wave cross sections. This is a remarkable result that could help to quantify the effect of two-nucleon knockout contributions to quasi-elastic neutrino-nucleus and anti-neutrino nucleus responses [34].

ACKNOWLEDGMENTS

This work is supported by the Research Foundation Flanders (FWO-Flanders) and by the Interuniversity Attraction Poles Programme P7/12 initiated by the Belgian Science Policy Office. The computational resources (Stevin Supercomputer Infrastructure) and services used in this work were provided by Ghent University, the Hercules Foundation

and the Flemish Government.

[1] R. B. Wiringa, R. Schiavilla, S. C. Pieper, and J. Carlson, Phys. Rev. C **89**, 024305 (2014), URL http://link.aps.org/doi/10.1103/PhysRevC.89.024305.

[2] A. Rios, A. Polls, and W. H. Dickhoff, Phys. Rev. C **89**, 044303 (2014), URL http://link.aps.org/doi/10.1103/PhysRevC.89.044303.

[3] J. Ryckebusch, W. Cosyn, and M. Vanhalst, J. Phys. **G42**, 055104 (2015), 1405.3814.

[4] K. S. Egiyan, N. Dashyan, M. Sargsian, S. Stepanyan, L. B. Weinstein, G. Adams, P. Ambrozewicz, E. Anciant, M. Anghinolfi, B. Asavapibhop, et al. (CLAS Collaboration), Phys. Rev. C **68**, 014313 (2003), nucl-ex/0301008, URL http://link.aps.org/doi/10.1103/PhysRevC.68.014313.

[5] K. S. Egiyan, N. B. Dashyan, M. M. Sargsian, M. I. Strikman, L. B. Weinstein, G. Adams, P. Ambrozewicz, M. Anghinolfi, B. Asavapibhop, G. Asryan, et al. (CLAS Collaboration), Phys. Rev. Lett. **96**, 082501 (2006), nucl-ex/0508026, URL http://link.aps.org/doi/10.1103/PhysRevLett.96.082501.

[6] N. Fomin, J. Arrington, R. Asaturyan, F. Benmokhtar, W. Boeglin, P. Bosted, A. Bruell, M. H. S. Bukhari, M. E. Christy, E. Chudakov, et al., Phys. Rev. Lett. **108**, 092502 (2012), 1107.3583, URL http://link.aps.org/doi/10.1103/PhysRevLett.108.092502.

[7] O. Hen, D. W. Higinbotham, G. A. Miller, E. Piasetzky, and L. B. Weinstein, Int. J. Mod. Phys. **E22**, 1330017 (2013), 1304.2813.

[8] G. Rosner, Prog. Part. Nucl. Phys. **44**, 99 (2000), ISSN 0146-6410, URL http://www.sciencedirect.com/science/article/pii/S0146641000000636.

[9] K. I. Blomqvist et al., Phys. Lett. B **421**, 71 (1998).

[10] C. J. G. Onderwater et al., Phys. Rev. Lett. **78**, 4893 (1997).

[11] C. J. G. Onderwater et al., Phys. Rev. Lett. **81**, 2213 (1998).

[12] R. Starink, M. van Batenburg, E. Cisbani, W. Dickhoff, S. Frullani, F. Garibaldi, C. Giusti, D. Groep, P. Heimberg, W. Hesselink, et al., Phys. Lett. B **474**, 33 (2000).

[13] J. Ryckebusch and W. Van Nespen, Eur. Phys. J. A **20**, 435 (2004), ISSN 1434-6001, URL http://dx.doi.org/10.1140/epja/i2003-10175-2.

[14] J. Ryckebusch, V. V. der Sluys, K. Heyde, H. Holvoet, W. V. Nespen, M. Waroquier, and M. Vanderhaeghen, Nucl. Phys. A **624**, 581 (1997), ISSN 0375-9474, URL http://www.sciencedirect.com/science/article/pii/S0375947497003850.

[15] C. Giusti, F. D. Pacati, K. Allaart, W. J. W. Geurts, W. H. Dickhoff, and H. Müther, Phys. Rev. C **57**, 1691 (1998), URL http://link.aps.org/doi/10.1103/PhysRevC.57.1691.

[16] A. Tang, J. W. Watson, J. Aclander, J. Alster, G. Asryan, Y. Averichev, D. Barton, V. Baturin, N. Bukhtoyarova, A. Carroll, et al., Phys. Rev. Lett. **90**, 042301 (2003), nucl-ex/0206003, URL http://link.aps.org/doi/10.1103/PhysRevLett.90.042301.

[17] R. A. Niyazov, L. B. Weinstein, G. Adams, P. Ambrozewicz, E. Anciant, M. Anghinolfi, B. Asavapibhop, G. Asryan, G. Audit, T. Auger, et al. (CLAS Collaboration), Phys. Rev. Lett. **92**, 052303 (2004), nucl-ex/0308013, URL http://link.aps.org/doi/10.1103/PhysRevLett.92.052303.

[18] R. Shneor, P. Monaghan, R. Subedi, B. D. Anderson, K. Aniol, J. Annand, J. Arrington, H. Benaoum, F. Benmokhtar, P. Bertin, et al. (Jefferson Lab Hall A Collaboration), Phys. Rev. Lett. **99**, 072501 (2007), nucl-ex/0703023, URL http://link.aps.org/doi/10.1103/PhysRevLett.99.072501.

[19] R. Subedi, R. Shneor, P. Monaghan, B. Anderson, K. Aniol, J. Annand, J. Arrington, H. Benaoum, F. Benmokhtar,

W. Boeglin, et al., Science **320**, 1476 (2008).

[20] I. Korover, N. Muangma, O. Hen, R. Shneor, V. Sulkosky, A. Kelleher, S. Gilad, D. W. Higinbotham, E. Piasetzky, J. W. Watson, et al. (Jefferson Lab Hall A Collaboration), Phys. Rev. Lett. **113**, 022501 (2014), URL http://link.aps.org/doi/10.1103/PhysRevLett.113.022501.

[21] O. Hen, M. Sargsian, L. B. Weinstein, E. Piasetzky, H. Hakobyan, D. W. Higinbotham, M. Braverman, W. K. Brooks, S. Gilad, K. P. Adhikari, et al., Science **346**, 614 (2014), http://www.sciencemag.org/content/346/6209/614.full.pdf, URL http://www.sciencemag.org/content/346/6209/614.abstract.

[22] C. Colle, W. Cosyn, J. Ryckebusch, and M. Vanhalst, Phys. Rev. C **89**, 024603 (2014), URL http://link.aps.org/doi/10.1103/PhysRevC.89.024603.

[23] Cosyn, Wim, Vanhalst, Maarten, and Ryckebusch, Jan, EPJ Web of Conferences **66**, 02022 (2014), URL http://dx.doi.org/10.1051/epjconf/20146602022.

[24] J. Ryckebusch, Phys. Lett. B **383**, 1 (1996), ISSN 0370-2693, URL http://www.sciencedirect.com/science/article/pii/0370269396007253.

[25] O. Hen, H. Hakobyan, R. Shneor, E. Piasetzky, L. Weinstein, W. Brooks, S. M.-T. Beck, S. Gilad, I. Korover, A. Beck, et al., Phys. Lett. B **722**, 63 (2013), ISSN 0370-2693, URL http://www.sciencedirect.com/science/article/pii/S0370269313002906.

[26] O. Hen and E. Piasetzky, (private communication).

[27] C. Colle, O. Hen, W. Cosyn, I. Korover, E. Piasetzky, J. Ryckebusch, and L. B. Weinstein, Phys. Rev. C **92**, 024604 (2015), URL http://link.aps.org/doi/10.1103/PhysRevC.92.024604.

[28] J. Ryckebusch, D. Debruyne, P. Lava, S. Janssen, B. Van Overmeire, and T. Van Cauteren, Nucl. Phys. A **728**, 226 (2003), nucl-th/0305066.

[29] W. Cosyn and J. Ryckebusch, Phys. Rev. C **87**, 064608 (2013), 1301.1904.

[30] R. J. Furnstahl, B. D. Serot, and H.-B. Tang, Nucl. Phys. A **615**, 441 (1997), nucl-th/9608035.

[31] M. Jain, M. L. Evans, G. Glass, J. C. Hiebert, R. A. Kenefick, L. C. Northcliffe, B. E. Bonner, J. E. Simmons, C. W. Bjork, P. J. Riley, et al., Phys. Rev. C **30**, 566 (1984), URL http://link.aps.org/doi/10.1103/PhysRevC.30.566.

[32] W. R. Gibbs and B. Loiseau, Phys. Rev. C **50**, 2742 (1994), URL http://link.aps.org/doi/10.1103/PhysRevC.50.2742.

[33] P. Lava, M. Martinez, J. Ryckebusch, J. Caballero, and J. Udias, Phys. Lett. B **595**, 177 (2004), ISSN 0370-2693, URL http://www.sciencedirect.com/science/article/pii/S0370269304007646.

[34] R. Acciarri, C. Adams, J. Asaadi, B. Baller, T. Bolton, C. Bromberg, F. Cavanna, E. Church, D. Edmunds, A. Ereditato, et al., Phys. Rev. D **90**, 012008 (2014), URL http://link.aps.org/doi/10.1103/PhysRevD.90.012008.

Appendix A: Qualitative model for the mass dependence of nuclear transparencies

In order to gain a qualitative understanding of the mass dependence of the transparency in knockout reactions we develop a toy model. In Sec. A 1 we introduce several scenarios each of which provides predictions for the mass dependence of the nuclear transparency. We display the numerical results in Sec. A 2.

1. Model

We model the nucleus as a homogeneous sphere with radius $R = 1.20A^{\frac{1}{3}}$ fm and constant density $\rho(\vec{r}) = 0.138$ fm^{-3}. Without attenuation the $A(e, e'N)$ cross section is proportional to the integrated density $\int \mathrm{d}^3\vec{r}\rho(\vec{r}) = A$. The atten-

uation with the nuclear medium is calculated with the aid of a classical survival probability $P(\vec{r})$. Given a nucleon brought into an energy continuum state at the coordinate $\vec{r}$, $P(\vec{r})$ is

$$P(\vec{r}) = \exp\left[-\sigma \int_z^{+\infty} \mathrm{d}z' \rho(\vec{r}')\right] . \tag{A1}$$

Let $\vec{r} = (x, y, z)$ and $\vec{r}' = (x, y, z')$. The integration variable z' runs along the direction of the momentum $\vec{p}$ of the outgoing nucleon. The cross section describing the scattering of the outgoing nucleon with the nuclear medium is denoted by σ. It is a measure for the aggregated effect of the attenuation. For a sphere with radius R and homogeneous density ρ the survival probability of Eq. (A1) becomes,

$$P(\vec{r}) = \exp\left[-\sigma\rho(\sqrt{R^2 - r^2\sin^2\xi} - r\cos^2\xi)\right] .$$

Here, ξ is the angle between $\vec{r}$ and $\vec{e}_p = \frac{\vec{p}}{p}$. The $A(e, e'N)$ nuclear transparency T_A^N, defined as the cross section including attenuation divided by the cross section without attenuation, is

$$T_A^N[\text{single}] \propto \frac{\int \mathrm{d}^2\Omega_p \int \mathrm{d}^3\vec{r}\rho(\vec{r})P(\vec{r})}{\int \mathrm{d}^2\Omega_p \int \mathrm{d}^3\vec{r}\rho(\vec{r})} = \frac{8\pi^2\rho \int_0^R \mathrm{d}r\, r^2 \int_{-1}^1 \mathrm{d}x \exp\left[-\sigma\rho(\sqrt{R^2 - r^2(1-x^2)} - rx)\right]}{4\pi A} . \tag{A2}$$

The integration $\int \mathrm{d}^2\Omega_p$ covers all possible outgoing-momentum directions.

For uncorrelated two-nucleon knockout the cross section is proportional to the total number of pairs $\int \mathrm{d}^3\vec{r}_1\rho(\vec{r}_1)$ $\int \mathrm{d}^3\vec{r}_2\rho(\vec{r}_2) = A^2$. The attenuation-corrected cross section is obtained by including the survival probability for both nucleons, and one finds for the two-nucleon knockout transparency $T_A^{NN}[\text{double}]$,

$$T_A^{NN}[\text{double}] \propto \frac{\int \mathrm{d}^2\Omega_{p_1} \int \mathrm{d}^3\vec{r}_1\rho(\vec{r}_1)P(\vec{r}_1) \int \mathrm{d}^2\Omega_{p_2} \int \mathrm{d}^3\vec{r}_2\rho(\vec{r}_2)P(\vec{r}_2)}{\int \mathrm{d}^2\Omega_{p_1} \int \mathrm{d}^3\vec{r}_1\rho(\vec{r}_1) \int \mathrm{d}^2\Omega_{p_2} \int \mathrm{d}^3\vec{r}_2\rho(\vec{r}_2)} = T_A^N[\text{single}] \cdot T_A^N[\text{single}] \tag{A3}$$

Next we investigate two-nucleon knockout in the ZRA, which serves as a proxy for identifying SRC-prone nucleon pairs. The ZRA is introduced by requiring that the initial nucleons are found at the same spatial coordinate. The cross section without attenuation is proportional to,

$$\int \mathrm{d}^2\Omega_{p_1} \int \mathrm{d}^2\Omega_{p_2} \int \mathrm{d}^3\vec{r}_1\rho(\vec{r}_1) \int \mathrm{d}^3\vec{r}_2\rho(\vec{r}_2)\delta(\vec{r}_1 - \vec{r}_2) = (4\pi)^2 \int \mathrm{d}^3\vec{r}\rho(\vec{r})^2 = (4\pi)^3\rho^2 \int_0^R \mathrm{d}r\, r^2 = (4\pi)^2\rho A \tag{A4}$$

We find that in the ZRA the two-nucleon knockout cross section is proportional to A as opposed to A^2 in the uncorrelated case. Including attenuation gives,

$$\int \mathrm{d}^3\vec{r}\rho(\vec{r})^2 \int \mathrm{d}^2\Omega_{p_1} P_1(\vec{r}) \int \mathrm{d}^2\Omega_{p_2} P_2(\vec{r}) = 16\pi^3\rho^2 \int_0^R \mathrm{d}r\, r^2 \int_{-1}^1 \mathrm{d}x \exp\left[-\sigma\rho(\sqrt{R^2 - r^2(1-x^2)} - rx)\right] \int_{-1}^1 \mathrm{d}y \exp\left[-\sigma\rho(\sqrt{R^2 - r^2(1-y^2)} - ry)\right] \tag{A5}$$

The transparency mass dependence is then given by the ratio of Eqs. (A5) and (A4),

$$T_A^{NN}[\text{ZRA}] \propto \frac{\pi\rho}{A} \int_0^R \mathrm{d}r\, r^2 \int_{-1}^1 \mathrm{d}x \exp\left[-\sigma\rho(\sqrt{R^2 - r^2(1-x^2)} - rx)\right] \int_{-1}^1 \mathrm{d}y \exp\left[-\sigma\rho(\sqrt{R^2 - r^2(1-y^2)} - ry)\right] \tag{A6}$$

It is well established that SRC pairs prefer back-to-back motion with anti-parallel momenta of the initial nucleon pair [16, 27]. After introducing the following angular constraints in the ZRA cross sections of Eqs. (A4),(A5),

$$\delta(\phi_1 - \phi_2 + \pi)\delta(\theta_1 + \theta_2 - \pi) ,$$

the transparency becomes,

$$T_A^{NN}[\text{ZRA+SRC}] \propto \frac{2\pi\rho}{A}\int_0^R \mathrm{d}r\, r^2 \int_{-1}^1 \mathrm{d}\cos\theta_1 \exp\left[-\sigma\rho(\sqrt{R^2-r^2(1-\cos^2\theta_1)}-r\cos\theta_1)\right] \tag{A7}$$

$$\times \int_{-1}^1 \mathrm{d}\cos\theta_2 \exp\left[-\sigma\rho(\sqrt{R^2-r^2(1-\cos^2\theta_2)}-r\cos\theta_2)\right]\delta(\theta_1+\theta_2-\pi)\,. \tag{A8}$$

With the substitution $(r,\cos\theta_1)\to(r,\ell=\sqrt{R^2-r^2(1-\cos^2\theta_1)})$, and further manipulations one finds,

$$T_A^{NN}[\text{ZRA+SRC}] \propto \frac{2\pi\rho}{A}\int_0^R \mathrm{d}\ell\,\ell\exp(-2\rho\sigma\ell)\sqrt{R^2-\ell^2}\ln\left(\frac{R+\ell}{R-\ell}\right)\,. \tag{A9}$$

2. Results

The mass dependence of the T_A^N, T_A^{NN} of Eqs. (A2),(A3),(A6),(A9) is investigated by varying the mass number A in the range $[12, 208]$. A power law is fitted to the numerical results $T_A \propto A^\lambda$. Figure 10 displays the numerical results for the exponent λ as a function of σ. In the limit of vanishing attenuation ($\sigma \to 0$) the cross section equals the plane-wave one and one has $T_A \approx A^0$.

For $\sigma > 10$ fm^2 we find that the λ values approach a limit value corresponding with an extremely opaque nucleus. In this limit one expects that the single-nucleon knockout cross section is surface dominated $\propto A^{\frac{2}{3}}$ as no nucleons originating from within the nucleus are able to escape. The mass dependence of $T_A^N[\text{single}]$ then becomes,

$$\lim_{\sigma\to+\infty} T_A^N[\text{single}] \propto \frac{A^{\frac{2}{3}}}{A} = A^{-\frac{1}{3}}\,, \tag{A10}$$

which complies with the measured value [25, 33]. For $T_A^{NN}[\text{double}]$, we have,

$$\lim_{\sigma\to+\infty} T_A^{NN}[\text{double}] = \lim_{\sigma\to+\infty} T_A^N[\text{single}]\cdot T_A^N[\text{single}] \propto A^{-\frac{2}{3}}\,. \tag{A11}$$

In the case of two-nucleon knockout in the ZRA the two nucleons originate from the same spatial coordinate. We again expect a surface dominated cross section as in the single nucleon knockout case, leading to the exponent $\lim_{\sigma\to+\infty}\lambda = -\frac{1}{3}$.

Including the additional constraint of back-to-back angles (ZRA+SRC in Fig. 10) will strongly favour the situation in which $(\vec{r}\perp\vec{e}_{p_1} \Leftrightarrow \vec{r}\perp\vec{e}_{p_2}) \wedge (r\approx R)$. When investigating the mass dependence of the transparency in the strong attenuation limit one finds (Fig. 10),

$$T_A^{NN}[\text{ZRA+SRC}] \propto \frac{A^0}{A^1} = A^{-1}\,. \tag{A12}$$

The cross section in the strong attenuation limit becomes **independent** of A.

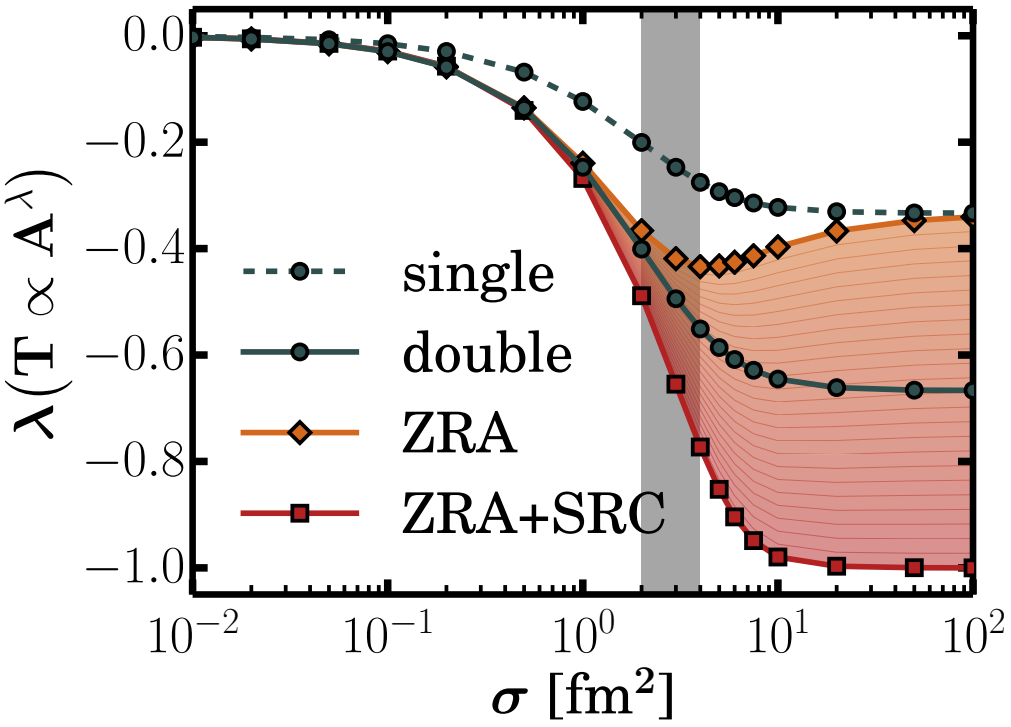

FIG. 10. (Color online) The exponents λ in $T_A^{N(N)} \propto A^{\lambda}$ as a function of the nucleon-nucleus cross section σ. The gray band corresponds with the σ of outgoing nucleon momenta $0.3 \leq p \leq 10$ GeV/c. With "single" we denote the T_A^N[single] results of Eq. (A2). With "double" we refer to the T_A^{NN}[double] results obtained with Eq. (A3) which corresponds to uncorrelated two-nucleon knockout. The "ZRA" ("ZRA+SRC") results for T_A^{NN}[ZRA] (T_A^{NN}[ZRA+SRC]) are obtained with the expressions of Eq. (A6)[Eq. (A9)].